MIP-based Electrochemical Protein Profiling

Lígia Bueno #[(1)], Hazim F. El-Sharif #[(2)], Maiara O. Salles #[(1)], Ryan D. Boehm[(3)], Roger J. Narayan[(3)], Thiago R. L. C. Paixão[(1)] and Subrayal M. Reddy[(2*)]

[1] Instituto de Quimica, Universidade de São Paulo, Avenida Professor Lineu Prestes, 748 – São Paulo – SP, Brasil.

[2] Department of Chemistry, FEPS, University of Surrey, Guildford, UK, GU2 7XH.

[3] Joint Departments of Biomedical Engineering, University of North Carolina, Raleigh, USA.

# These authors contributed equally to this work (co-first authorship)

***Corresponding Author:** Tel: +44 (0) 1483686396, s.reddy@surrey.ac.uk

Graphical Abstract

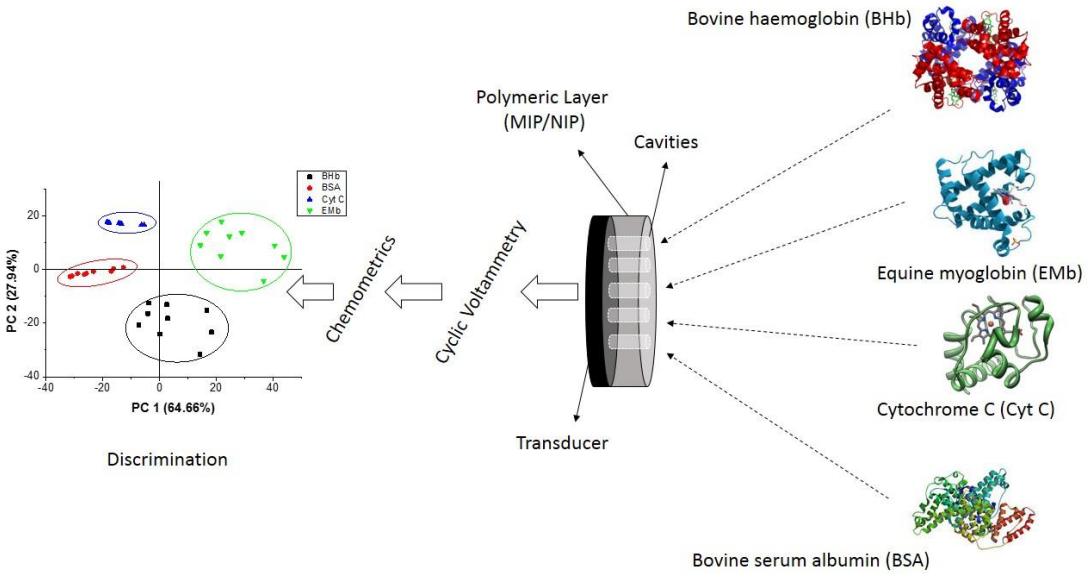

Highlights

- Electrochemical MIP-based biosensor fabricated for rapid protein detection.
- We report the coupling of electrochemical and pattern recognition techniques.
- Selective synthetic MIP recognition of a range of bio-significant proteins.
- Protein fingerprint profiling by principal component analysis
- Faster detection rates at lower concentrations.

Abstract

We present the development of an electrochemical biosensor based on modified glassy carbon (GC) electrodes using hydrogel-based molecularly imprinted polymers (MIPs) has been fabricated for protein detection. The coupling of pattern recognition techniques via principal component analysis (PCA) has resulted in unique protein fingerprints for corresponding protein templates, allowing for MIP-based protein profiling. Polyacrylamide MIPs for memory imprinting of bovine haemoglobin (BHb), equine myoglobin (EMb), cytochrome C (Cyt C), and bovine serum albumin (BSA), alongside a non-imprinted polymer (NIP) control, were spectrophotometrically, and electrochemically characterised using modified GC electrodes. Rebinding capacities (Q) were revealed to be higher for larger proteins (BHb and BSA, $Q \approx 4.5$) while (EMb and Cyt C, $Q \approx 2.5$). Electrochemical results show that due to the selective nature of MIPs, protein arrival at the electrode via diffusion is delayed, in comparison to a NIP, by attractive selective interactions with exposed MIP cavities. However, at lower concentrations such discriminations are difficult due to low levels of MIP rebinding. PCA loading plots revealed 5 variables responsible for the separation of the proteins; E_p, I_p, $E_{1/2}$, $I_{at\ -0.8\ V}$, $\Delta I_{decay\ peak\ current\ to\ -0.8\ V}$. Statistical symmetric measures of agreement using Cohen's kappa coefficient (κ) were revealed to be 63% for bare GC, 96% for NIP and 100% for MIP. Therefore, our results show that with the use of PCA such discriminations are achievable, also with the advantage of faster detection rates. The possibilities for this MIP technology once fully developed are vast, including uses in bio-sample clean-up or selective extraction, replacement of biological antibodies in immunoassays, as well as biosensors for medicine, food and the environment.

Keywords

Biosensors; Electrochemical protein detection; Molecularly imprinted polymers; Pattern recognition; Modified electrodes; Electronic tongue.

1. Introduction

Molecularly imprinted polymers (MIPs) are rapidly becoming viable alternatives to natural antibodies for sensor technology [1-4]. MIPs offer many advantages in terms of shelf-life, stability, robustness, cost, and ease of preparation [5]. While biological antibodies are routinely used in diagnostic tests and are able to give precise results, they are notably unstable and require lengthy procedures to grow, isolate, and treat before they can be used; ethical issues surrounding the use of animal-based antibodies are also a common drawback [6].

Over the years molecular imprinting has become an effective method for imprinting highly specific and selective recognition sites in synthetic polymers [7,8]. As such, MIPs have been regarded as 'antibody mimics' and have shown clear advantages over actual antibodies for sensor technology as they are highly cross-linked, intrinsically stable, robust, and have potential use in extreme environments [9]. However, in the imprinting community, bio-macromolecules such as proteins present a variety of challenges and successful imprints are highly sought after. Proteins are relatively labile and have changeable conformations that are sensitive to various factors (e.g., solvent environments, pH and temperature) [7,10-12]. Moreover, a large number of proteins are vital markers; for example, in the case of haemoglobin, mutations in genes that encode for the protein's subunits can result in hereditary diseases such as *sickle cell anaemia, thalassaemia,* and *haemoglobinopathies* [1]. However, protein-detecting arrays remain under-developed due to the lack of highly

selective and specific binding agents that interact with protein surfaces through complementary interactions [13]. It is therefore imperative to develop new methodologies based on protein detection for applications in proteomics, medical diagnostics, and even pathogen detection [13].

Differential receptor arrays, that in nature routinely conduct pattern-based recognition, have already been artificially constructed using synthetic receptors/transducers and could provide a possible solution. Such devices have been labelled as electronic noses for smell recognition and electronic tongues for taste recognition. These synthetic receptors/transducers or sensors have low selectivity and consequently exhibit over-lapping signals for different species, providing a fingerprint of a sample that could be used for qualitative discrimination [14]. The operation of these electronic devices uses a concept of the human tongue and nose known as global selectivity [15], in which the biological system does not identify a particular substance but brings together all of the extracted information into patterns that the brain decodes. An electronic sensor that works in a similar way is a chememotric tool e.g., principal component analysis (PCA). These tools decode complex information and classify standards for recognition [16-18]. Takeuchi et al. previously applied the electronic tongue strategy to the molecular recognition of proteins by using imprinted acrylic acid (AA) and 2-dimethylaminoethyl methacrylate (DMA) polymers [19,20]. Three-dimensional PCA scores of the binding data described by Takeuchi et al. revealed that a clear protein distinction was possible and that protein-imprinted polymer arrays can be applied to protein profiling by pattern analysis of binding activity for each polymer [19-21]. PCA has also been used in conjunction with electrochemical methods such as cyclic voltammetry [16,17,22-25]. An attractive

approach for the development of biochemical sensors would be the integration of smart materials (e.g., MIPs) with said electrochemical techniques

This paper demonstrates the use of pattern recognition techniques to uniquely identify fingerprint profiles for four different proteins by coupling electrochemical sensor strategies with hydrogel-based MIPs. The four proteins chosen were on the basis of their different biological roles, sizes, and electrochemical activities. Bovine hemoglobin (BHb, 64.5 kda) well known for its function in the vascular system as a carrier of oxygen, also in aiding the transport of carbon dioxide and regulating blood pH [26]. Both BHb and EMb (17.5 kda) exhibit well-known electrochemical behaviour [1,24,27,28]. Cytochrome complex (Cyt C, 12.5 kda) is an essential component of the electron transport chain but exhibits a lack of oxygen binding, despite being an iron-containing metalloprotein that is capable of undergoing oxidation and reduction. Bovine serum albumin (BSA, MW 66.0 kDa) is a non-metalloprotein with similar molecular weight to BHb, and serves to test the selectivity of the BHb-MIP to BSA compared to template BHb.

Our results demonstrate sensitivity and selectivity; if such devices can be further optimised for MIP parameters, then perhaps these MIP-based strategies can offer viable methods for the characterisation of proteins. With the aid of inexpensive synthetic smart material hydrogel MIPs, new biosensor platforms for rapid screening, diagnosis, and monitoring of a variety of disorders can be readily developed within the years to come [8,29].

2. Materials and methods

2.1 Materials

Acrylamide (AA), N,N-methylenebisacrylamide (bis-AA), ammonium persulphate (APS), N,N,N,N-tetramethylethyldiamine (TEMED), sodium dodecyl-sulphate (SDS), glacial acetic acid (AcOH), phosphate buffered saline (PBS) tablets (137 mmol L^{-1} NaCl; 27 mmol L^{-1} KCl; 10 mmol L^{-1} Na_2HPO_4; 1.76 mmol L^{-1} KH_2PO_4), methyl viologen, bovine haemoglobin (BHb), bovine serum albumin (BSA), cytochrome C (Cyt C), and equine heart myoglobin (EMb) were all purchased from Sigma-Aldrich (Poole, UK). Sieves (75µm) were purchased from Inoxia Ltd. (Guildford, UK). Polycarbonate membranes 25 mm in diameter, 0.8 µm pore size were purchased from Osmonic Inc., Minnetonka, USA.

2.2 Hydrogel production

Hydrogel MIPs for BHb, EMb, Cyt C and BSA were synthesised by separately dissolving AA (54 mg) and bis-AA as cross-linker (6 mg) along with template protein (12 mg) in 960 µL of MilliQ water. The solutions were purged with nitrogen for 5 minutes, followed by an addition of 20 µL of a 10% (w/v) APS solution and 20 µL of a 5% (v/v) TEMED solution. Polymerisation occurred at room temperature (~22 C^0), giving final total gel densities (%T) of 6 %T, AA/bis-AA (w/v) and crosslinking densities (%C) of 10 %C (9:1, w/w). For every MIP created, a control non-imprinted polymer (NIP) was prepared in an identical manner but in the absence of protein.

2.3 Hydrogel conditioning

After polymerization, the gels were granulated separately using a 75 µm sieve. Of the resulting gels, 500 mg were conditioned by washing with five 1 mL volumes of 150 mmol L^{-1} PBS buffer (pH 7.4). This was followed by five 1 mL volumes of a 10% (w/v):10% (v/v) SDS:AcOH (pH 2.8). A further five 1 mL washes of 150 mmol

L^{-1} PBS buffer (pH 7.4) were conducted to remove any residual SDS:AcOH eluent and equilibrate the gels. Each conditioning step was followed by a centrifugation using an Eppendorf mini-spin plus centrifuge (Fisher Scientific, Loughborough, UK) for 3 minutes at 6000 rpm (RCF: 2419 x g). All supernatants were collected for analysis by spectrophotometry to verify the extent of template removal. It should be noted that the last water wash and SDS:AcOH eluent fractions were not observed to contain any protein. Therefore we are confident that any remaining template protein within the MIPs did not continue to leach out during future studies.

2.4 Hydrogel characterization

The rebinding efficiency of the MIPs and NIPs produced were characterized using a UV mini-1240 CE spectrophotometer (Shimadzu Europa, Milton Keynes, UK). After elution washing of the polymers MIP and NIP (500 mg) were treated with 3 mg/ml of protein in an eppendorf and polymer/protein solution mixed on a rotary vortex mixer for 5 minutes followed by centrifugation. The supernatant was removed and protein concentration measured spectrophotometrically (at 404 nm for BHb; 280 nm for BSA, 408 nm for Mb and 402 nm for Cyt C). Protein loaded MIPs and NIPs were then washed with five sequential washes of water (1ml each) and the washes combined. Again the absorbance of the washes was also taken. All protein unaccounted for at this stage was deemed to be selectively bound to the MIP or NIP and determined by subtraction of the protein levels in supernatants (after loading and water washing) from the initial load. Optical microscope images of granulated and washed MIPs and NIPs were also taken.

2.5 Electrochemical analysis

Glassy carbon (GC) working electrode surfaces were individually modified with a 20 mg conditioned hydrogel layer of each: NIP, BHb MIP, Cyt C MIP, BSA MIP, and EMb MIP. The layer was kept in place by a polycarbonate membrane (0.8 µm) placed over the modified electrode surface and held down with the aid of a rubber ring. The polycarbonate membrane was chosen because its pores are small enough to retain the gel (75 µm particle size) and, at the same time, large enough to allow protein in solution to diffuse through. The potential range used in all electrochemical measurements was 0.0 to -0.9 V with a scan rate of 100 mV s^{-1}; a Ag/AgCl reference electrode (saturated KCl) and platinum counter electrode connected to an Autolab II potentiostat/galvanostat were used in this study (Utrecht, Netherlands). The modified electrodes were first placed in a solution of PBS (pH 7.4) and SDS 5% (w/v) and analysed after a 20 min period of equilibration. Subsequently, 15.4 µmol L^{-1} protein solutions (BHb, BSA, EMb and Cyt C) dissolved in PBS buffer (pH 7.4) and SDS 5% (w/v) were placed independently in the cell and voltammograms were obtained at 10 min intervals for 60 min. It should be noted that protein solutions were stirred between measurements for 3 minutes; GC electrodes were cleaned, polished, and tested with methyl viologen between each new MIP/NIP experiment. Cyclic voltammograms using bare GC electrodes were also recorded for the PBS (pH 7.4) and SDS 5% (w/v) buffer solution and for the 15.4 µmol L^{-1} protein solutions (BHb, BSA, EMb and Cyt C) dissolved in PBS buffer (pH 7.4) and SDS 5% (w/v).

2.6 Principal component analysis

Principal component analysis (PCA) and hierarchical cluster analysis (HCA) were performed in Statistica 11.0 (StatSoft Inc., Tulsa, USA). The analysis was

carried out using voltammetric current density values without any previously pre-processing and scaling from bare GC or modified GC electrodes as input. PCA was used to reduce the large data sets to 2D plots, which can be easily used to discriminate protein samples. All voltammetric curves were recorded three times for each sample in a random order using a clean bare GC or a new modified GC electrode surface.

3. Results and discussion

3.1 Characterisation

Figure 1A and 1B show the optical microscope images of granulated and washed BHb MIPs and NIPs. The MIPs appear denser than the NIPs due to the light contrast apparent from protein which is still locked in the bulk of the MIP. It is also evident that the MIP particles form larger agglomerates with each other compared with the NIP. This is because there is still surface entrapped protein in the MIP particles which is attracted to more surface entrapped protein within other MIP particles. This is not observed with the NIP.

The molecular imprinting effect is characterised by the rebinding capacity (Q) of protein to the gel polymer (mg/g) exhibited by the protein-specific MIP and the control NIP, and is calculated using Eq. (1), where C_i and C_r are the initial protein and the recovered protein concentrations (mg/ml) respectively (which specifies the specific protein bound within the gel), V is the volume of the initial solution (ml), and g is the mass of the gel polymers (g).

$$Q = [C_i - C_r]\, V/g \qquad (1)$$

Figure 1C shows the rebinding capacities for each protein studied. As expected, the MIP exhibited superior selective binding of the target protein compared with the NIP with a typical selectivity ratio of 10:1. Interestingly, the binding capacity

222 is highest for BHb-MIP_{polyAA} while both EMb-MIP_{polyAA} and BCat- MIP_{polyAA} exhibit
223 the lowest binding capacity. It has previously been observed that with smaller size
224 proteins a higher crosslinking density is necessary; the opposite is also true for larger
225 proteins [12,30]. Since the crosslinking density remained the same (10% by weight),
226 the low MIP affinities for BCat and EMb can be attributed to the fact that fewer
227 cavities were imprinted due too high, and too low of a crosslinking density
228 respectively.
229
230 **3.2 Electrochemical analysis**
231 *3.2 .1 Glassy carbon (GC) profiling*
232 Metallo-proteins are expected to produce an electrochemical signal because of
233 their metal-containing haem active centres in the protein molecules. However, the
234 extended three-dimensional structure of proteins results in the inaccessibility of the
235 electroactive iron centres. It can therefore be difficult for metallo-proteins to undergo
236 heterogeneous electron transfer; as a result, no detectable current appears at
237 conventional electrodes [1,4]. However, conformational changes due to partial or
238 complete protein denaturation, can allow haem groups to become accessible to a
239 subjacent electrode and be electrochemically reduced at GC electrodes via promotion
240 of electrocatalytic reduction of nascent oxygen [1]. For example, conformational or
241 structural changes in oxyhaemoglobin (Hb) complexes can be induced upon
242 denaturation in the presence of sodium dodecylsulphate (SDS) denaturant [1,11,31].
243 With this in mind, we attempted to evaluate the possibility to discriminate the
244 proteins using cyclic voltammetric information extracted from bare GC electrodes in
245 the presence of an SDS surfactant in solution. Cyclic voltammograms were recorded
246 in the presence of the four proteins that were studied at 15.4 μmol L^{-1} (including one

247 non-metalloprotein as a control; BHb - 1 mg mL^{-1}, BSA - 0.98 mg mL^{-1}, EMb - 0.26
248 mg mL^{-1}, and Cyt C - 0.185 mg mL^{-1}) in a solution containing PBS buffer (pH 7.4)
249 and 5% SDS (w/v) (Figure 2A). In the presence of Cyt C and BSA, the cathodic
250 reduction signal of dissolved oxygen in solution could be seen (reduction peak at -0.6
251 V). The fact that the peak was due to dissolved oxygen was confirmed by bubbling
252 Ar in the latter protein solutions, which consequently led to depletion of the oxygen
253 reduction peak (results not shown). In the presence of BHb and EMb, a shift in the
254 peak reduction potential towards a less negative potential was observed, indicating an
255 iron centre-dependent electrocatalytic process for the oxygen reduction reaction at the
256 surface of the electrode. This effect was not observed in the absence of SDS, and is
257 therefore due to a probable SDS–induced change in the haemoglobin and myoglobin
258 structural conformation exposing the Fe(III) centre by partial denaturation. The
259 partial denaturation is induced only by SDS where at 5% (w/v) the CMC is reached.
260 Full denaturation however, requires a combination of SDS surfactant and an acid in
261 order to protonate the protein and hence be further attracted to and unravelled by
262 negatively charged SDS micelles [31]. With this modification, the reduction of the
263 oxygen does not directly happen at the electrode surface; the Fe(III) is reduced to
264 Fe(II) at the electrode surface and the oxygen reduction is subsequently
265 electrocatalysed by the oxidation of Fe(II) back to Fe(III).

266 Using hierarchical cluster analysis (HCA) the qualitative discrimination of the
267 proteins on the GC electrode was performed and data were analysed for their
268 discrimination and compiled as number of cluster recognition (Figure 2B). The results
269 reveal that a slight degree of separation between the proteins that, in solution, exhibit
270 and do not exhibit a shift in the peak reduction potential of the oxygen
271 electrochemical process, as clearly observed in the voltammetric profile. However,

further evaluation of the recognized sample similarities shows that the model using data extract with a bare electrode was unable to clearly discriminate individual proteins inside the groups of protein clusters.

3.2.2 Hydrogel profiling

That the MIP can detect partially denatured protein is of significance to the exploitation of this electrochemical technique in protein discrimination. Indeed Kryscico *et al.* recently demonstrated using CD spectroscopy that during the imprinting process, some of the protein undergoes conformational changes and is partially denatured [32,33]. The MIPs therefore are imprinted with both native as well as partially denatured protein. The MIPs and NIPs were therefore analysed electrochemically with SDS treated protein to give partially denatured protein.

Considering the selective nature of MIPs, protein arrival at the electrode surface via diffusion should be delayed by the MIP due to attractive selective interactions with exposed cavities [1]. With this in mind, GC electrode surfaces were individually modified with a conditioned hydrogel layer (20 mg) of BHb MIP, EMb MIP, Cyc C MIP, and BSA MIP.

To ensure the successful elution of protein from the MIP (and thus confirming the presence of selective cavities through conditioning), BHb MIPs at different stages were tested electrochemically on the electrode. Figure 3A characterizes the cyclic voltammograms for freshly prepared MIP (with BHb still in the cavities; referred to as MIP1), the same MIP washed to remove protein (referred to as MIP2) and also NIP. The results clearly demonstrate that the MIP loaded with protein exhibits similar electrochemistry to the BHb solution in Figure 2A. The reduction peak observed at around -0.4V is the iron mediated reduction of oxygen. This suggests that the GC

297 electrode is able to detect the protein at the surface due to the ‘un-eluted’ MIP’s
298 presence and concurred with previously reported electrochemical MIP studies [1].
299 Conversely, when protein is not present in either the MIP or the NIP, the
300 electrochemistry (reduction peak at -0.6 V) reverts to direct electrochemical reduction
301 of dissolved oxygen.

302 Protein diffusion through MIP and NIP layers was initially studied at 154 and
303 15.4 μmol L^{-1}. Whereas the NIP response time remained constant at 10 min for all
304 protein concentrations, we found that the MIP response time decreases from our
305 previously reported 40 min [1] to 10 min at low protein concentrations. Figure 3B
306 illustrates the resulting voltammograms for 0 and 10 minutes of BHb exposure at 15.4
307 μmol L^{-1} using a modified BHb-MIP layer (20 mg). It can be seen that a shift in the
308 peak reduction potential for the oxygen reduction was observed after only 10 min of
309 BHb exposure. Therefore, both MIP and NIP share the same reduced response time at
310 lower concentrations. This result suggests that the template protein exhibits little
311 interaction with the MIP cavities at the lower concentrations, which is associated with
312 a less tortuous path to the electrode. It could be that at low protein concentrations we
313 observe extensive protein denaturation in the presence of SDS and therefore there is
314 little or no interaction between denatured protein and the mixed population of MIP
315 cavities for native and partially denatured protein.

316 Another possibility is that the ‘template’ forms a mixed population of free and
317 clustered proteins when the template is imprinted at a very high concentration (12 mg
318 mL^{-1}). The resultant population of imprinted sites would therefore contain some
319 cavities that are associated with protein clusters. This phenomenon is supported by
320 our previous work [34,35], where force spectroscopy analysis of MIPs suggested that
321 the cavities accommodated an agglomeration of template protein molecules rather

than just a single molecule. It is therefore possible that the solution phase represents a more dispersed protein population compared with the original imprinted template population for rebinding protein at low concentrations. If the cavities only respond to a critical number of protein molecules in a given arrangement, then this could explain why the MIP does not appear to be selective at low protein concentrations.

However, although the presence of SDS in solution (5% (w/v)) allows for protein detection at the electrode by iron exposure, it also implies that MIP recognition within the specific cavities may technically not be able to rebind the partially denatured and unfolded protein structures due to an altered size and shape. In light of this, recent studies have shown that when imprinting a mixture of stable and partially denatured proteins are present [9,32,33].Therefore it is still possible that the MIPs can function as a recognition element and rebind a small percentage of the heterogeneous protein configurations.

In order to confirm these assumptions and elucidate the hypothesis that MIP cavities undergo an electrochemical discrimination of their template proteins, individually modified GC electrodes with all four hydrogel MIP layers were separately tested across all four proteins. Cyclic voltammograms for all MIP were recorded in a solution containing PBS (pH 7.4), SDS 5% (w/v), and 15.4 μmol L^{-1} of the four proteins for different times of protein exposure (0-60 minutes). It was noted that the current signal for both BHb and EMb at 15.4 μmol L^{-1} achieved steady state behaviour after 10 minutes, indicating that this time could be used for all further measurements. Therefore, using the voltammetric current density values PCA score plots for each MIP and protein combination were plotted at 10 minutes of protein exposure.

Figure 4A illustrates the average PCA score plot for the four MIPs as they all shared the same cluster separation. A clear discrimination and separation (using 92.9 % of the original information) of the four proteins clusters at 10 min of protein exposure can be seen. This indicated that MIP cavity interactions could play an important role in the discrimination process. Of the four different clusters, Cyt C and BSA clusters are far less scattered than BHb and EMb clusters. An explanation for this behaviour could be ascribed to the fact that the BHb MIP was selective for both BHb and EMb (which bear similarities in their structure), allowing for them to bind in the MIP cavities and consequently making the diffusion rate less reproducible in the MIP. The separation for Cyt C and BSA can be justified due to their adsorption at GC electrode surfaces, subsequently changing the rate of the oxygen reduction. A change in the peak current and in the current decay from peak current to -0.8 V ($\Delta I_{\text{decay peak current to -0.8 V}}$) for the oxygen reduction was observed for all the experiments with Cyt C and BSA proteins when compared with a blank solution. These adsorption rates of Cyt C and BSA can be related to previously published values [27,36]. It is plausible that this adsorption effect and delayed diffusion due to MIP cavity interactions are responsible for the discrimination process [37]. PCA loading plots revealed the variables responsible for the separation of the proteins; 5 variables could be elected: E_p, I_p, $E_{1/2}$, $I_{\text{at -0.8 V}}$, $\Delta I_{\text{decay peak current to -0.8 V}}$.

Thus, the effective diffusion rate of proteins through the composite membranes could be a function of specific and non-specific cavities of the polymeric MIP layer [37]. Therefore, the time of protein diffusion was considered an important parameter for the discrimination process. This indicated that GC electrodes modified with an acrylamide cavity-based MIP could be used as a sensor to discriminate different kinds of proteins at 10 minutes of protein exposure. However, mechanical

obstruction of the polymeric layer using a control non-imprinted polymer (NIP) on the GC electrode surface was conducted in order to validate the MIP-protein rebinding profiles. This allows only for the non-specificity of the polymeric layer to be evaluated due to the lack of selective cavities. All discrimination experiments were executed identically as reported using the MIP layers; the only altered variable was the modified NIP layer (20 mg). Unfortunately, PCA plots revealed NIP to have similar protein discrimination (Figure 4B) to that of a MIP at 10 minutes of protein exposure. Therefore only the protein diffusion rate through the polymeric layer could be considered as a possible discriminating factor for the four proteins.

A closer look at the PCA data using interpreted HCA data compiled as number of cluster recognition reveals that the four proteins are best profiled using both MIP and NIP layers (Figure 5A and B, respectively) when compared with bare GC electrode (Figure 2B). The symmetric measures between our protein discrimination models, in terms of a percentage measurement of agreement using Cohen's kappa coefficient (κ), are illustrated in Table 1. Since the approx. significance (*p)* = .000 (which actually means $p < .0005$), our κ coefficients are statistically significantly different from zero (63% for bare GC, 96% for NIP and 100% for MIP). Therefore, there is a clear comparison between the behavioural models for protein discrimination.

Furthermore, clustering relationships for each of the four proteins are apparent; this phenomenon is especially noticeable in the MIP and NIP PCA plots (Figure 4). It should be noted that in different studies, involving bare GC electrodes, MIP modified GC electrodes or NIP modified GC electrodes, all PCA protein clusters fall into the same pattern recognition, thus providing an overall cohesive protein profile. Each protein retains its own individual cluster within a single quadrant of the

PCA plot. Interestingly, our studies illustrate that proteins with a metal center behave similarly; it can clearly be seen that both metalloproteins that exhibit a peak potential shift (BHb and EMb) are on the right half of the vector, while BSA and Cyt C are on the other. Moreover, the smaller sized proteins (EMB ~17.5kDa and Cyt C ~12.5kDa) are on the top half of the plot. This recognition approach could be useful for future protein speciation profiling.

4. Conclusions

The proposed electrochemical and PCA coupled method proved to be efficient for discriminating four proteins (BHb, Mb, BSA and Cyt C), indicating that glassy carbon (GC) electrodes modified with either a MIP or NIP layer could be used as a fast sensor to discriminate between different kinds of proteins. At high concentrations, the selective nature and integrity of MIPs delays the protein response and leads to an obvious difference between MIP and NIP performance. At lower concentrations, such discriminations are difficult due to an apparent lack of critical protein agglomeration and/or complete denaturation of protein molecules impeding optimum protein binding within cavities. With the use of PCA, protein discrimination has been achievable at faster detection rates. Our results suggest that PCA could be used to interrogate and discriminate between proteins when hydrogels are integrated to electrochemical sensors.

Acknowledgements

The authors are grateful to the University Global Partnership Network (Universities of Surrey, Sao Paulo and NC State), The Royal Society, NERC, ACTF of the RSC, FAPESP (Fundação de Amparo à Pesquisa do Estado de São Paulo;

Grant Numbers: 2012/12106-5, 2011/11115-8, 2011/23355-3), CAPES (Coordenação de Aperfeiçoamento de Pessoal de Nível Superior), and CNPq (Conselho Nacional de Desenvolvimento Científico e Tecnológico; Grant Numbers: 470919/2011-6 and 302700/2011-0) for financial support.

The authors would also like to thank Dr PJ McCabe (Clinical Res Centre) at the University of Surrey for his contributions towards the statistical evaluation of this work.

References

[1] S.M. Reddy, G. Sette, Q. Phan, Electrochemical probing of selective haemoglobin binding in hydrogel-based molecularly imprinted polymers, Electrochim. Acta. 56 (2011) 9203-9208.

[2] H. Chen, Z. Zhang, R. Cai, X. Chen, Y. Liu, W. Rao, S. Yao, Molecularly imprinted electrochemical sensor based on amine group modified graphene covalently linked electrode for 4-nonylphenol detection, Talanta. 115 (2013) 222-227.

[3] B. Khadro, C. Sanglar, A. Bonhomme, A. Errachid, N. Jaffrezic-Renault, Molecularly imprinted polymers (MIP) based electrochemical sensor for detection of urea and creatinine, Procedia Engineering. 5 (2010) 371-374.

[4] X. Kan, Z. Xing, A. Zhu, Z. Zhao, G. Xu, C. Li, H. Zhou, Molecularly imprinted polymers based electrochemical sensor for bovine hemoglobin recognition, Sensors Actuators B: Chem. 168 (2012) 395-401.

[5] S.A. Piletsky, N.W. Turner, P. Laitenberger, Molecularly imprinted polymers in clinical diagnostics—Future potential and existing problems, Med. Eng. Phys. 28 (2006) 971-977.

[6] V.J.B. Ruigrok, M. Levisson, M.H.M. Eppink, H. Smidt, J. van der Oost, Alternative affinity tools: more attractive than antibodies? Biochem. J. 436 (2011) 1-13.

[7] M.E. Byrne, V. Salian, Molecular imprinting within hydrogels II: Progress and analysis of the field, Int. J. Pharm. 364 (2008) 188-212.

[8] P.A. Lieberzeit, R. Samardzic, K. Kotova, M. Hussain, MIP Sensors on the Way to Biotech Application: Selectivity and Ruggedness, Procedia Engineering. 47 (2012) 534-537.

[9] D.R. Kryscio, N.A. Peppas, Critical review and perspective of macromolecularly imprinted polymers, Acta Biomaterialia. 8 (2012) 461-473.

[10] S.M. Reddy, D.M. Hawkins, Q.T. Phan, D. Stevenson, K. Warriner, Protein detection using hydrogel-based molecularly imprinted polymers integrated with dual polarisation interferometry, Sensors Actuators B: Chem. 176 (2013) 190-197.

[11] E. Verheyen, J.P. Schillemans, M. van Wijk, M. Demeniex, W.E. Hennink, C.F. van Nostrum, Challenges for the effective molecular imprinting of proteins, Biomaterials. 32 (2011) 3008-3020.

[12] H.F. El-Sharif, Q.T. Phan, S.M. Reddy, Enhanced selectivity of hydrogel-based molecularly imprinted polymers (HydroMIPs) following buffer conditioning, Anal. Chim. Acta. 809 (2014) 155-161.

[13] H.C. Zhou, L. Baldini, J. Hong, A.J. Wilson, A.D. Hamilton, Pattern recognition of proteins based on an array of functionalized porphyrins, J. Am. Chem. Soc. 128 (2006) 2421-2425.

[14] Y. Vlasov, A. Legin, A. Rudnitskaya, C. Di Natale, A. D'Amico, Nonspecific sensor arrays ("electronic tongue") for chemical analysis of liquids (IUPAC Technical Report), Pure and Applied Chemistry. 77 (2005) 1965-1983.

[15] K. Toko, Taste sensor with global selectivity, Materials Science & Engineering C-Biomimetic Materials Sensors and Systems. 4 (1996) 69-82.

[16] J. Zeravik, A. Hlavacek, K. Lacina, P. Skládal, State of the Art in the Field of Electronic and Bioelectronic Tongues ? Towards the Analysis of Wines, Electroanalysis. 21 (2009) 2509-2520.

[17] E.A. Baldwin, J. Bai, A. Plotto, S. Dea, Electronic Noses and Tongues: Applications for the Food and Pharmaceutical Industries, Sensors. 11 (2011) 4744-4766.

[18] C. Baggiani, L. Anfossi, C. Giovannoli, C. Tozzi, Multivariate analysis of the selectivity for a pentachlorophenol-imprinted polymer, Journal of Chromatography B. 804 (2004) 31-41.

[19] T. Takeuchi, D. Goto, H. Shinmori, Protein profiling by protein imprinted polymer array, Analyst. 132 (2007) 101-103.

[20] T. Takeuchi, T. Hishiya, Molecular imprinting of proteins emerging as a tool for protein recognition, Organic & Biomolecular Chemistry. 6 (2008) 2459.

[21] K.D. Shimizu, C.J. Stephenson, Molecularly imprinted polymer sensor arrays, Curr. Opin. Chem. Biol. 14 (2010) 743-750.

[22] T.R.L.C. Paixao, M. Bertotti, Fabrication of disposable voltammetric electronic tongues by using Prussian Blue films electrodeposited onto CD-R gold surfaces and recognition of milk adulteration, Sensors and Actuators B-Chemical. 137 (2009) 266-273.

[23] M.O. Salles, M. Bertotti, T.R.L.C. Paixao, Use of a gold microelectrode for discrimination of gunshot residues, Sensors and Actuators B-Chemical. 166 (2012) 848-852.

494 [24] W. Novakowski, M. Bertotti, T.R.L.C. Paixao, Use of copper and gold electrodes
495 as sensitive elements for fabrication of an electronic tongue: Discrimination of wines
496 and whiskies, Microchemical Journal. 99 (2011) 145-151.

497 [25] L. Bueno, R.L.C. Paixão Thiago, A Single Platinum Microelectrode for
498 Identifying Soft Drink Samples, International Journal of Electrochemistry. 2012
499 (2012) 1-5.

500 [26] Q. Gai, F. Qu, Y. Zhang, The Preparation of BHb-Molecularly Imprinted Gel
501 Polymers and Its Selectivity Comparison to BHb and BSA, Sep. Sci. Technol. 45
502 (2010) 2394-2399.

503 [27] S. Boussaad, N.J. Tao, R. Zhang, T. Hopson, L.A. Nagahara, In situ detection of
504 cytochrome c adsorption with single walled carbon nanotube device, Chem. Commun.
505 0 (2003) 1502-1503.

506 [28] S. Wu, W. Tan, H. Xu, Protein molecularly imprinted polyacrylamide membrane:
507 for hemoglobin sensing, Analyst. 135 (2010) 2523-2527.

508 [29] M.J. Whitcombe, I. Chianella, L. Larcombe, S.A. Piletsky, J. Noble, R. Porter, A.
509 Horgan, The rational development of molecularly imprinted polymer-based sensors
510 for protein detection, Chem. Soc. Rev. 40 (2011) 1547-1571.

511 [30] D.E. Hansen, Recent developments in the molecular imprinting of proteins,
512 Biomaterials. 28 (2007) 4178-4191.

513 [31] D.M. Hawkins, D. Stevenson, S.M. Reddy, Investigation of protein imprinting in
514 hydrogel-based molecularly imprinted polymers (HydroMIPs), Anal. Chim. Acta. 542
515 (2005) 61-65.

[32] D.R. Kryscio, M.Q. Fleming, N.A. Peppas, Conformational studies of common protein templates in macromolecularly imprinted polymers, Biomed. Microdevices. 14 (2012) 679-687.

[33] D.R. Kryscio, M.Q. Fleming, N.A. Peppas, Protein Conformational Studies for Macromolecularly Imprinted Polymers, Macromolecular Bioscience. 12 (2012) 1137-1144.

[34] E. Saridakis, S. Khurshid, L. Govada, Q. Phan, D. Hawkins, G.V. Crichlow, E. Lolis, S.M. Reddy, N.E. Chayen, Protein crystallization facilitated by molecularly imprinted polymers, Proceedings of the National Academy of Sciences. 108 (2011) 11081-11086.

[35] H. EL-Sharif, D.M. Hawkins, D. Stevenson, S.M. Reddy, Determination of protein binding affinities within hydrogel-based molecularly imprinted polymers (HydroMIPs), Phys. Chem. Chem. Phys. 16 (2014) 15483-15489.

[36] X. Zhao, R. Liu, Z. Chi, Y. Teng, P. Qin, New Insights into the Behavior of Bovine Serum Albumin Adsorbed onto Carbon Nanotubes: Comprehensive Spectroscopic Studies, J Phys Chem B. 114 (2010) 5625-5631.

[37] R. Schirhagl, U. Latif, D. Podlipna, H. Blumenstock, F.L. Dickert, Natural and Biomimetic Materials for the Detection of Insulin, Anal. Chem. 84 (2012) 3908-3913.

Table captions

Table 1 - Symmetric Measures; Cohen's kappa coefficient (κ) as a percentage measurement of agreement, asymptotic std. error not assuming the null hypothesis[a], approximate T as the ratio of κ to the asymptotic standard error assuming the null hypothesis[b], and the approximate statistical significance (p).

Figure captions

Figure 1 - Microscope imaging of 75µm hydrogel particles: (A) non-imprinted control (NIP); (B) bovine haemoglobin (BHb) imprinted MIP_{polyAA}. (C) Rebinding capacities and imprinting effects of MIP_{polyAA} and NIP_{polyAA} for several biological molecules (bovine haemoglobin (BHb), bovine serum albumin (BSA), myoglobin (Mb), Cytochrom C (Cyt C)). Data represents mean ± S.E.M., $n = 3$.

Figure 2 – (A) Cyclic voltammograms recorded in PBS (pH 7.4), SDS 5% (w/v), and in the presence of protein in solution (15.4 µmol L^{-1}) (cytochrome C (a), bovine serum albumin (b), equine heart myoglobin (c) and bovine haemoglobin (d)). Scan rate: 100 mV s^{-1}. Electrode: bare glassy carbon (GC) electrode. (B) Cluster analysis percentage prediction scores for the four proteins using GC electrodes.

Figure 3 - Cyclic voltammograms recorded in PBS (pH 7.4), SDS 5% (w/v), and in the presence of BHb in solution (15.4 µmol L^{-1}) at scan rate of 100 mV s^{-1}: (A) Glassy carbon (GC) electrode modified with hydrogel layers of NIP (a), unconditioned BHb-MIP1 (b), conditioned BHb-MIP2 (c) after 0 minutes of protein exposure. (B) Glassy carbon (GC) electrode modified with hydrogel layer of BHb MIP. Measurement made after 0 (a) and 10 (b) minutes of protein exposure.

Figure 4 - PCA score plots: (A) glassy carbon (GC) electrode modified with hydrogel MIP layer, results show the average response of all four different MIPs; (B) glassy carbon (GC) electrode modified with a non-imprinted hydrogel layer. Voltammetric

569 date recorded in PBS (pH 7.4), SDS 5% (w/v), and in the presence of each protein
570 (15.4 µmol L^{-1}). Potential programme employed to record the voltammetric curves
571 used as input to perform PCA: E_i=0.0 V, E_{V1}=-0.9 V, E_f = 0.0 V, and scan rate = 100
572 mV s^{-1}. Measurement made after 10 minutes of protein exposure.
573
574 Figure 5 - Cluster analysis percentage prediction scores for the four proteins; (A) MIP
575 modified GC electrodes, (B) NIP modified GC electrodes.
576

577 Table 1

Model	κ (%)	Asymp. Std. Error[a]	Approx. T[b]	Approx. Sig. (ρ)
Bare GCE	63%	0.1	6.543	0.00
NIP	96%	0.036	10.018	0.00
Mb MIP	100%	0	10.392	0.00
Cyt C MIP	100%	0	10.392	0.00
BSA MIP	100%	0	10.392	0.00
BHb MIP	96%	0.04	9.414	0.00

578

579

580

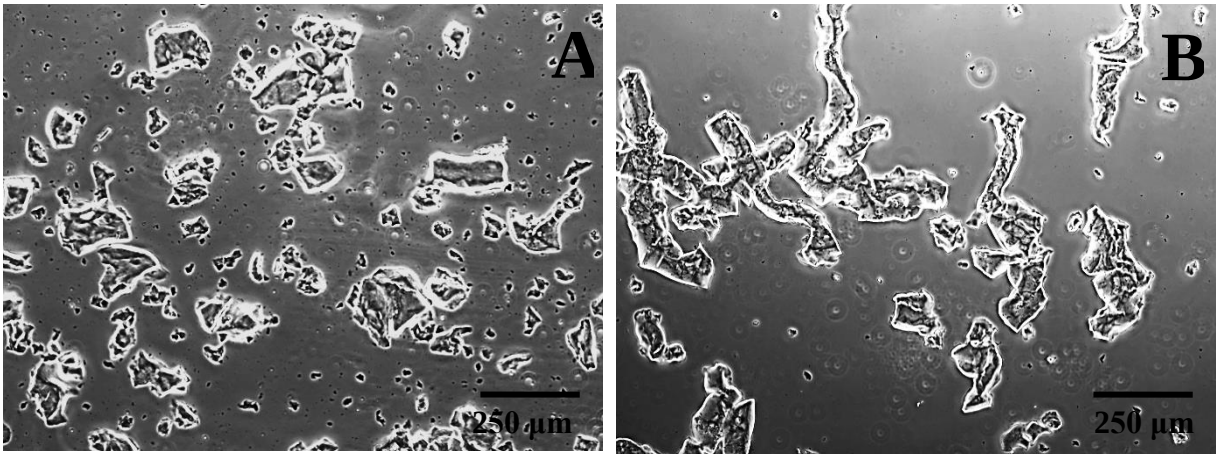

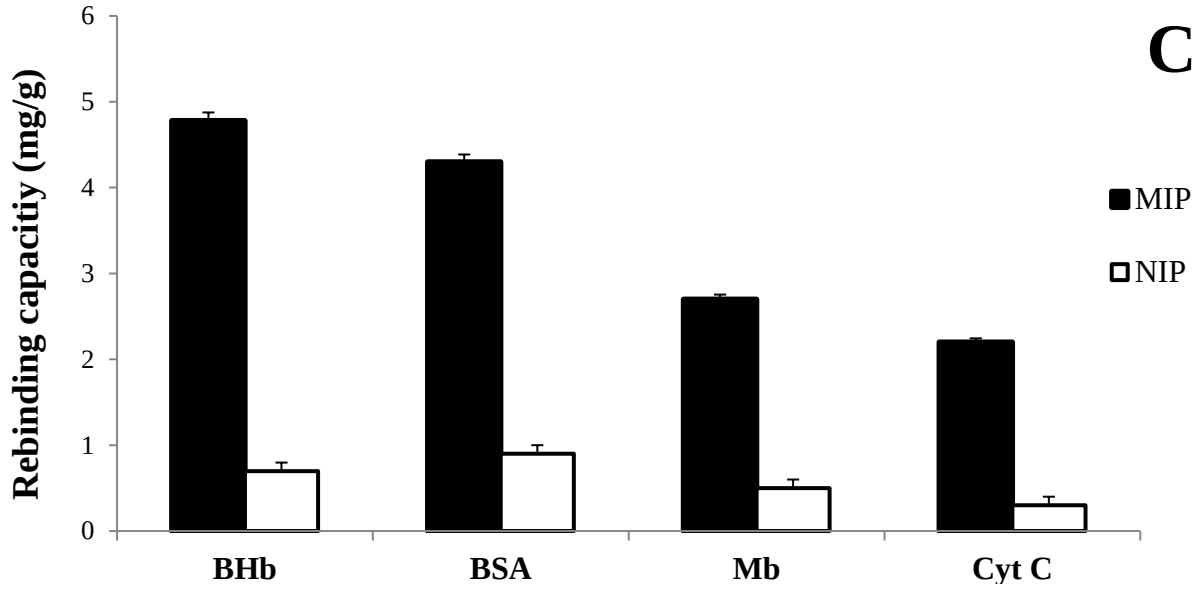

581

582 Figure 1

583

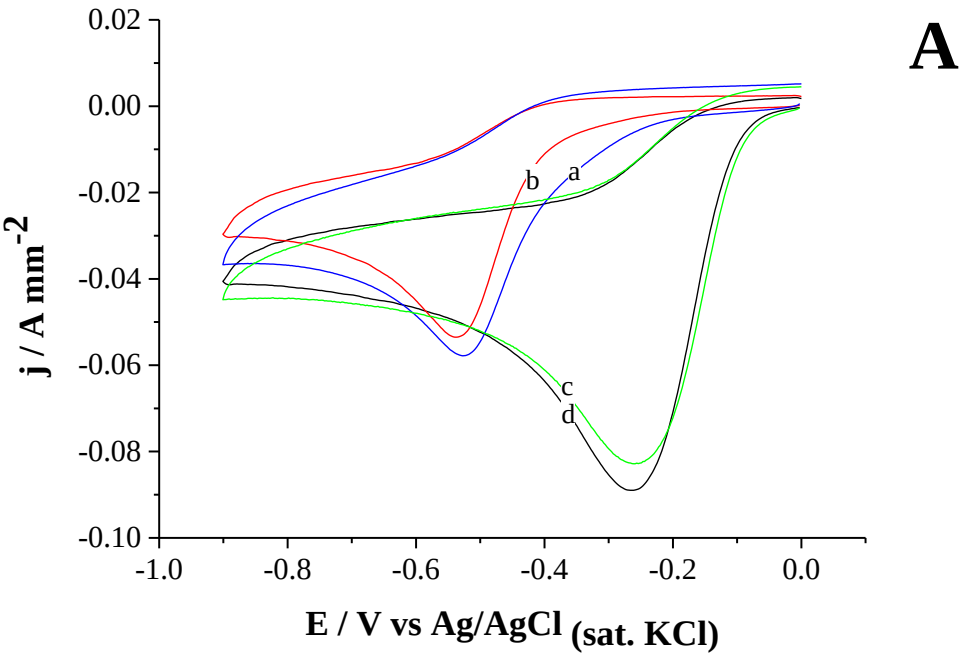

584

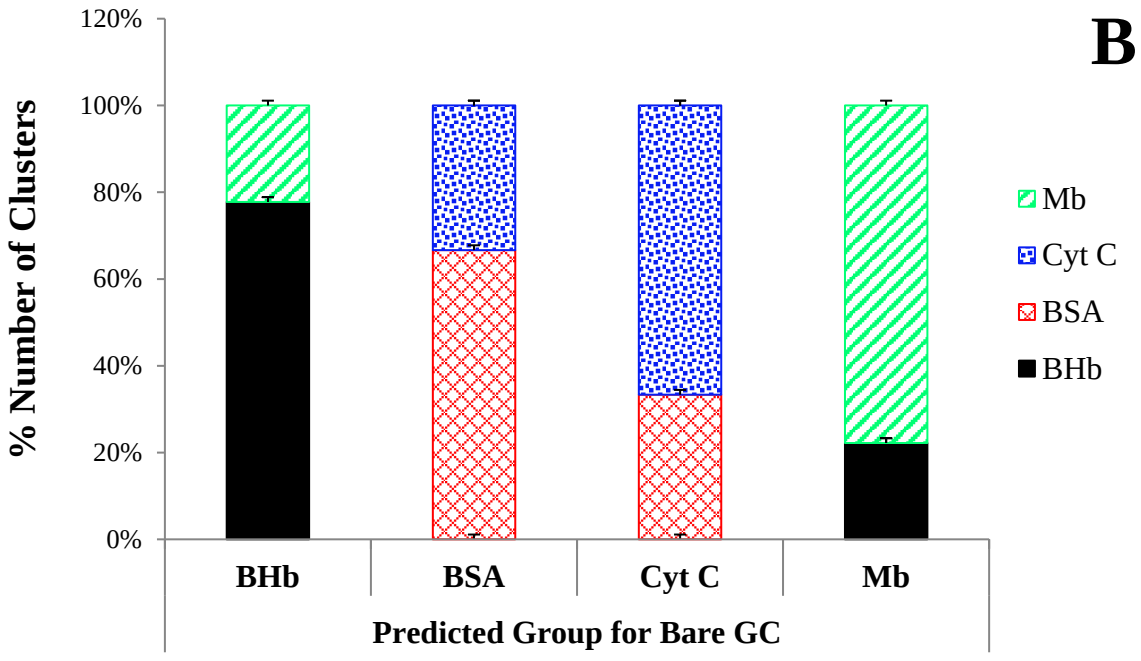

585

586 Figure 2

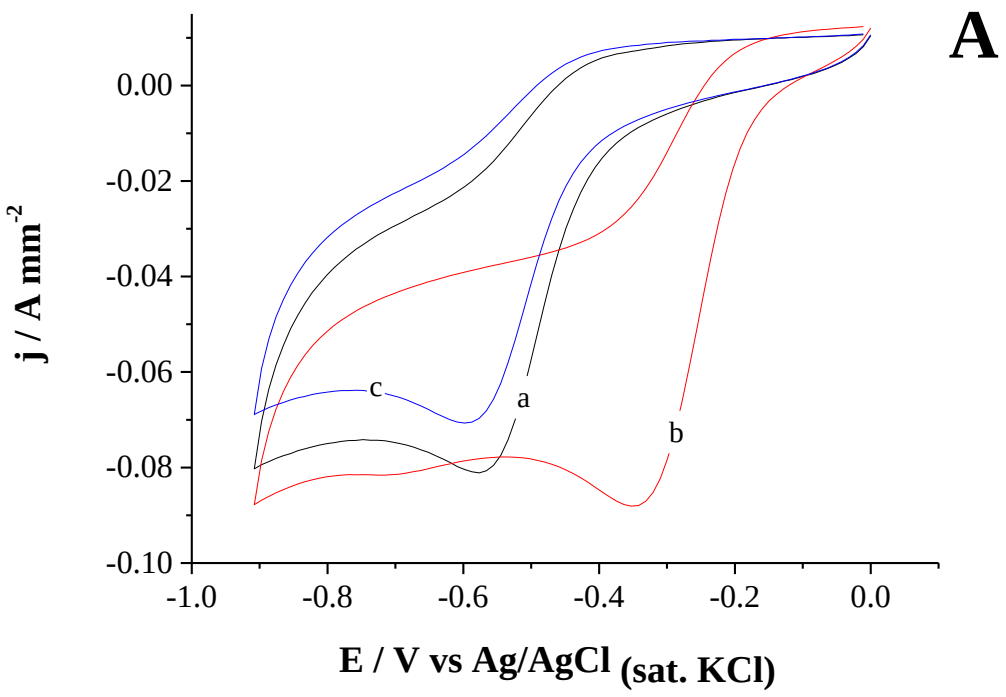

587

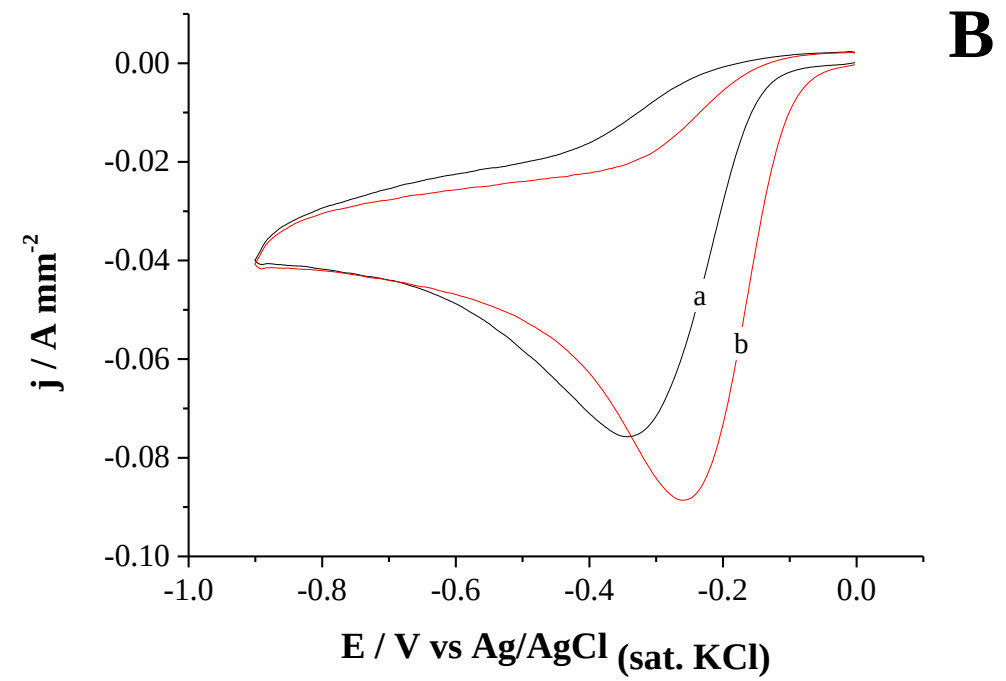

588
589 Figure 3

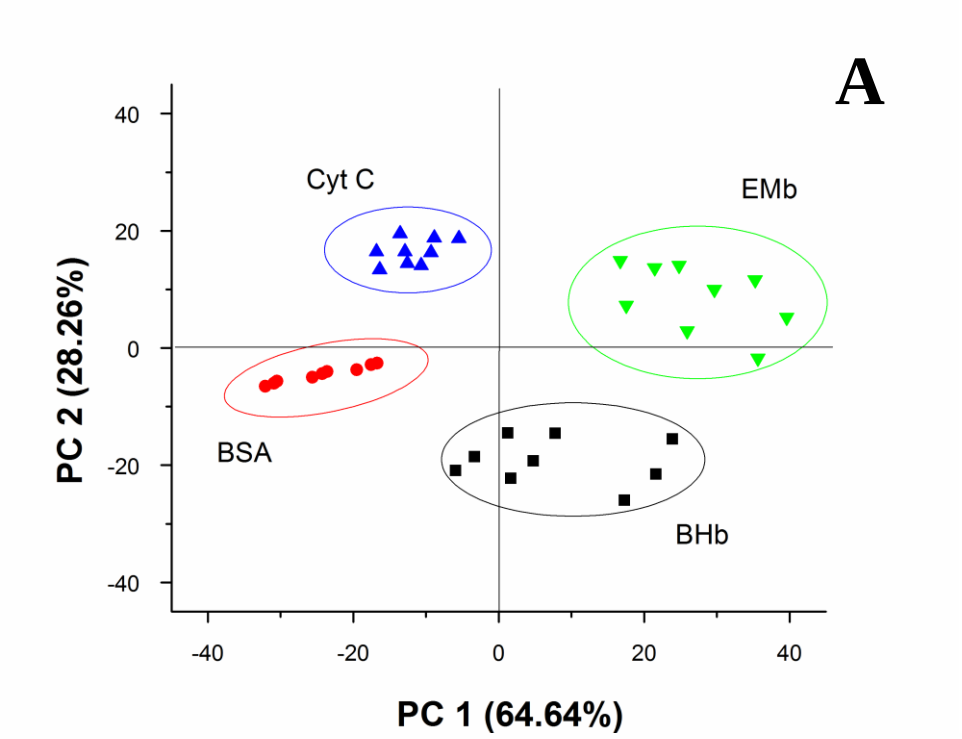

590

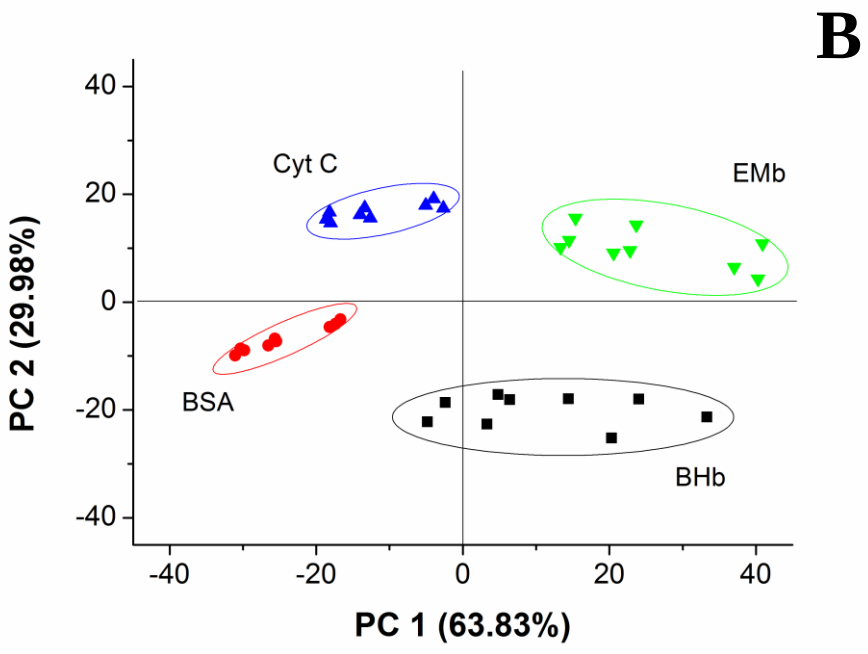

591

592 Figure 4
593

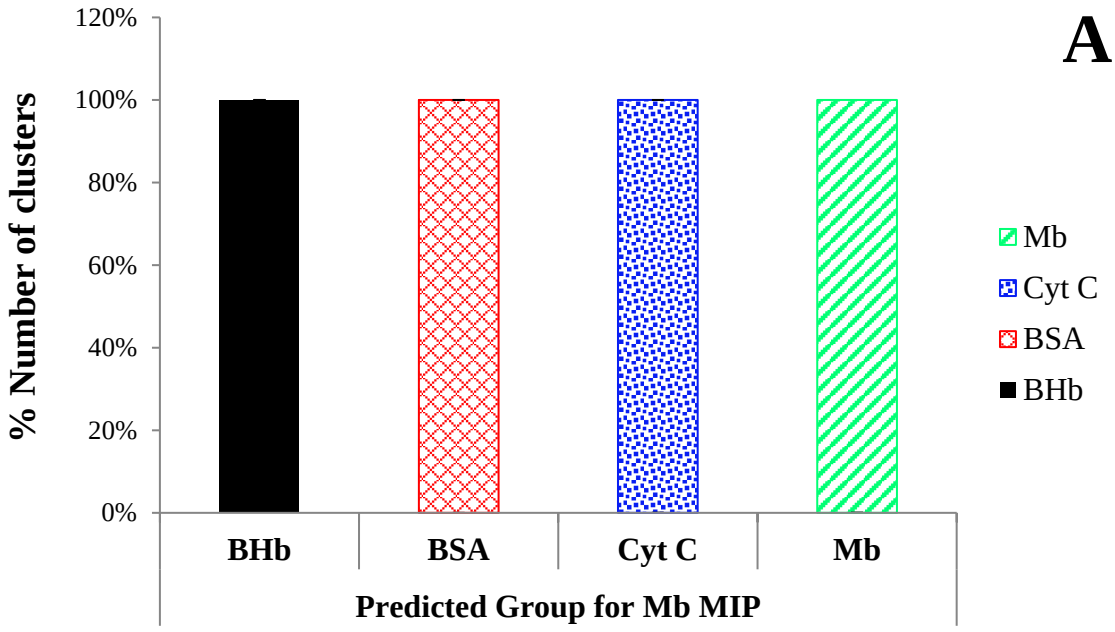

594

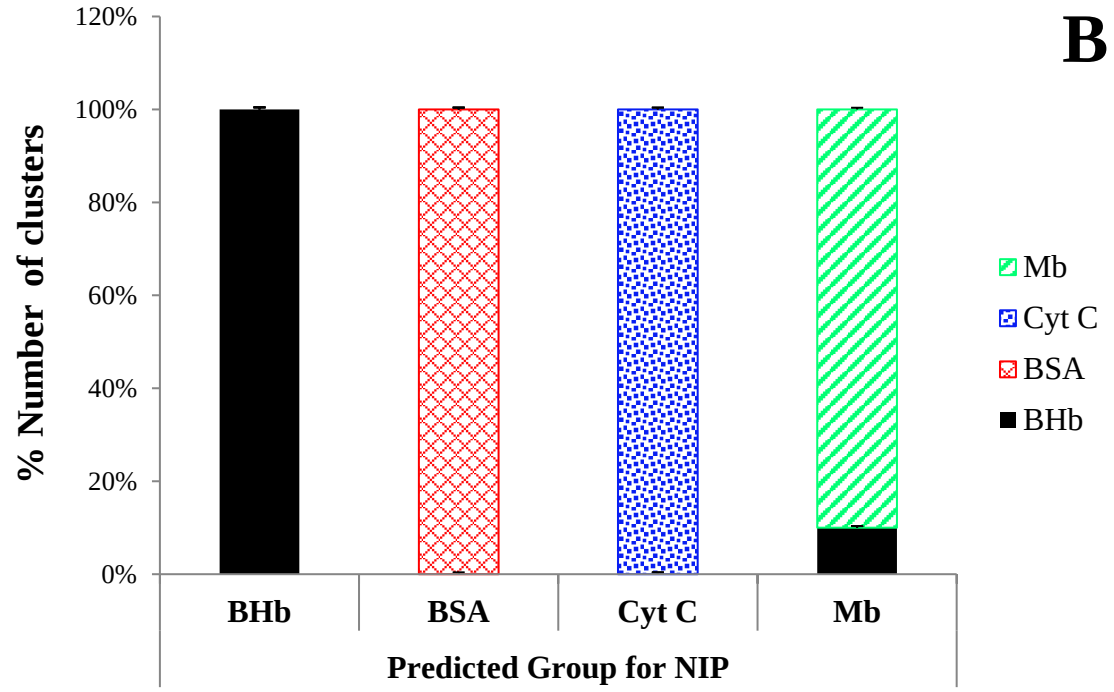

595

596

597 Figure 5

598